

An angular-momentum preserving dissipative model for the point-mass N -body problem

Matheus Lazarotto^{1*} and Clodoaldo Ragazzo¹

^{1*}Instituto de Matemática, Estatística e Ciências da Computação,
Universidade de São Paulo, São Paulo, 05508-090, SP, Brasil.

*Corresponding e-mail: m.j.lazarotto@gmail.com;

Abstract

A simple mathematical model emulating energy dissipation due to tidal effects is proposed. In this model, forces acting between masses remove energy but preserve the total angular momentum of the system. We study the effect of such forces on a particular family of orbits, namely those corresponding to central configurations, and show that a specific dependence on the mutual distances between the bodies leads to homographic equations equivalent to those of the two-body problem with dissipation. We then describe in detail the topology of solutions of the dissipative two-body system via Poincaré compactification. Finally, we present equations averaged over Keplerian motion showing no influence of the dissipation on periapsis precession.

Keywords: Celestial Mechanics, N -body problem, Dissipative systems, Transient dynamics

1 Introduction

When predicting the fate of N -bodies mutually attracted by gravity, two main frameworks are often used to model their dynamical evolution. In the conservative one, orbits are either regular (periodic or quasi-periodic) or chaotic, where bodies may escape, collide, or revolve around each other indefinitely [1–3]. In the dissipative one, these scenarios can still occur, but pairs of bounded bodies, given sufficient time, eventually end up in spin-orbit coupling, facing each other while moving in circular orbits, or collide [4].

In fact, the spin-orbit coupling among bounded pairs extends to systems with any number of bodies ($N > 2$), as the whole system is progressively reduced, pair by pair, to one of the final states described: escapes, collisions, or synchronizations [5].

In detail, one can start by assuming the conservative dynamics for N -bodies, generally taking place on the hypersurface $E : \mathbb{R}^{3N} \times T\mathbb{R}^{3N} \rightarrow \mathbb{R}$, corresponding to the system's mechanical energy

$$E(\mathbf{r}, \dot{\mathbf{r}}) = T(\dot{\mathbf{r}}) + U(\mathbf{r}), \quad (1)$$

for $\mathbf{r} = (\mathbf{r}_1 \dots \mathbf{r}_N) = (x_1 \ y_1 \ z_1 \ \dots \ x_N \ y_N \ z_N) \in \mathbb{R}^{3N}$ as the cartesian position for all N -bodies, and $\dot{\mathbf{r}} = \frac{d\mathbf{r}}{dt} \in T\mathbb{R}^{3N}$ as their velocities. The kinetic energy

$$T(\dot{\mathbf{r}}) = \frac{1}{2} \sum_{i=1}^N m_i (\dot{\mathbf{r}}_i \cdot \dot{\mathbf{r}}_i) \quad (2)$$

and the gravitational potential energy

$$U(\mathbf{r}) = -G \sum_{i=1}^{N-1} \sum_{j=i+1}^N \frac{m_i m_j}{|\mathbf{r}_{ij}|}, \quad (3)$$

are computed for masses m_i with relative distances $\mathbf{r}_{ij} = \mathbf{r}_i - \mathbf{r}_j \in \mathbb{R}^3$.

If no external forces act on the system, and regardless of internal constraints, the dynamics will preserve both the energy function (1) and the total angular momentum

$$\mathbf{L} = \sum_{i=1}^N m_i (\mathbf{r}_i \times \dot{\mathbf{r}}_i), \quad (4)$$

due to the central nature of the forces from the gravitational potential (3). The expressions (1) to (4) hold for a reference frame fixed at and moving with the center of mass of the whole system, satisfying

$$\sum_{i=1}^N m_i \mathbf{r}_i = \sum_{i=1}^N m_i \dot{\mathbf{r}}_i = 0. \quad (5)$$

In this context, Smale [1] proved that for any gravitational system of point-masses, the critical points of the energy function (1) restricted to a constant angular momentum (4) hypersurface correspond to relative equilibrium configurations, i.e.,

$$\frac{d|\mathbf{r}_{ij}|}{dt} = 0 \quad \forall i, j. \quad (6)$$

On top of that, Moeckel [6] showed that for $N > 2$ any relative equilibrium is a saddle-point of the energy function, when restricted to a constant angular momentum level. Later, Moeckel [7] proved similar results for systems of interacting rigid bodies.

In the presence of tides, which dissipates energy but not angular momentum, many dynamical conclusions can be derived from the results of Smale and Moeckel. For instance, for $N \geq 2$, energy dissipation leads to two possible physical scenarios: either bodies collide and/or move apart and ultimately become isolated masses; or, after successive collisions and escapes, pairs of masses remain in circular motion, where no further energy can be dissipated. See [5, 8] for details. The combination of Smale’s and Moeckel’s results assert that, despite the existence of relative equilibria, their instability prevents systems with more than two bodies to remain in such states indefinitely.

It is well known that the behavior observed in nature is dissipative, as different mechanisms act on any group of celestial bodies due to internal friction (tidal effects), several types of drag (motion within gases, dust, plasma, etc.), and radiative effects [3]. However, in empty space, these dissipative forces are generally weak, and the timescales required to reach final states are often unattainable. As a result, one typically observes systems in transient configurations lasting for millions or even billions of years, closely resembling stability. This suggests that the nature of dissipative effects allows for prolonged transients near semi-equilibrium states, making them relevant to the dynamical evolution as such states likely represent most of a system’s lifetime and determine their path toward any final state it may reach.

Several models for dissipative effects have been studied [9–14], mainly involving Poynting-Robertson drag, solar wind, atmospheric drag, or surface contact. In these cases, dissipation typically acts as a drag force opposing the body’s velocity through a damping term $-\alpha\dot{\mathbf{r}}$ in the equation of motion

$$m\ddot{\mathbf{r}} = -\alpha\dot{\mathbf{r}} - \nabla U(\mathbf{r}). \quad (7)$$

Even though these models correspond to relevant and realistic scenarios, they remove both energy and angular momentum from the system. By contrast, at planetary scale, the most prominent dissipative effect is gravitational in origin, arising from tides [15, 16], which preserves angular momentum.

In this context, we introduce a simple model for dissipation between celestial bodies that, while dissipating energy, preserves angular momentum. This is achieved by introducing a central damping force that breaks time symmetry while maintaining rotational symmetry.

We remark that a force similar, though not identical, to the one we propose has already appeared in a PhD thesis by Chong Ai under the supervision of Mark Levi [17]. Since their force dissipates energy while preserving angular momentum, their qualitative results for the dissipative Kepler problem are similar to ours. They also studied dissipative effects in the restricted three-body problem, an investigation that we are also pursuing. To our knowledge, the exact force expression we propose, which under dissipation leaves invariant a surface that in the conservative case is generated by the homographic solutions, has not been proposed before.

In what follows, we present the model and its main properties in Section 2. Section 3 discusses its effects on planar central configurations, while Section 4 and 5 provide

topological and numerical results for the simpler case of two bodies – results that also apply to planar central motions for any number of bodies.

2 Model

To incorporate energy dissipation while conserving angular momentum, we draw on Mignard’s tidal force approximation for two nearly spherical bodies (eq. (5) in [18]). We simplify his expression to a point-mass scenario by neglecting rotational terms, yielding the dissipative force $\mathbf{f}_{\text{diss}}^{ij}$ between a pair of masses m_i and m_j

$$\mathbf{f}_{\text{diss}}^{ij}(\dot{\mathbf{r}}_{ij}, \mathbf{r}_{ij}) = -\alpha \frac{Gm_i m_j}{|\mathbf{r}_{ij}|^d} (\dot{\mathbf{r}}_{ij} \cdot \hat{\mathbf{r}}_{ij}) \hat{\mathbf{r}}_{ij}, \quad (8)$$

where $\hat{\mathbf{r}}_{ij} = \frac{\mathbf{r}_i - \mathbf{r}_j}{|\mathbf{r}_i - \mathbf{r}_j|} \in \mathbb{R}^3$ is the versor connecting the i -th and j -th bodies. The dissipation strength α is constant and has units of $[L^{d-3}T]$. Physically, it reflects rheological and viscoelastic effects, carrying the dependence on the body’s Love number (deviation from a spherical shape), equatorial radius, and tidal torque delay¹. Since the current study prioritizes a mathematical approach, we treat the radial dependence exponent d as a free parameter, as it will be discussed further in the text. Physically, a direct comparison to Mignard’s model would yield $d = 8$.

The force (8) is pairwise anti-symmetric ($\mathbf{f}_{ij} = -\mathbf{f}_{ji}$), dissipative because it depends on the relative velocity ($\dot{\mathbf{r}}_{ij} = \dot{\mathbf{r}}_i - \dot{\mathbf{r}}_j$), and central ($\mathbf{f}_{ij} \parallel \hat{\mathbf{r}}_{ij}$). It is also homogeneous in the positions and velocities $\mathbf{f}_{\text{diss}}^{ij}(\nu \dot{\mathbf{r}}_{ij}, \mu \mathbf{r}_{ij}) = \nu \mu^{-d} \mathbf{f}_{\text{diss}}^{ij}(\dot{\mathbf{r}}_{ij}, \mathbf{r}_{ij})$.

We start by considering the conservative Lagrangian for N point masses

$$\mathcal{L} = \frac{1}{2} \sum_{i=1}^N m_i (\dot{\mathbf{r}}_i \cdot \dot{\mathbf{r}}_i) + G \sum_{i=1}^{N-1} \sum_{j=i+1}^N \frac{m_i m_j}{|\mathbf{r}_{ij}|}, \quad (9)$$

and introduce dissipation via the Rayleigh function

$$\mathcal{D} = \frac{\alpha}{2} \sum_{i=1}^{N-1} \sum_{j=i+1}^N \frac{Gm_i m_j}{|\mathbf{r}_{ij}|^d} (\dot{\mathbf{r}}_{ij} \cdot \hat{\mathbf{r}}_{ij})^2, \quad (10)$$

which modify the Euler-Lagrange equations as

$$\frac{d}{dt} (\nabla_{\dot{\mathbf{r}}_i} \mathcal{L}) = \nabla_{\mathbf{r}_i} \mathcal{L} - \nabla_{\dot{\mathbf{r}}_i} \mathcal{D}; \quad (11)$$

yielding the equations of motion

¹ In principle, the dissipation constant α may vary from body to body, so that

$$\mathbf{f}_{\text{diss}}^{ij}(\dot{\mathbf{r}}_{ij}, \mathbf{r}_{ij}) = -\alpha_i \alpha_j \frac{Gm_i m_j}{|\mathbf{r}_{ij}|^d} (\dot{\mathbf{r}}_{ij} \cdot \hat{\mathbf{r}}_{ij}) \hat{\mathbf{r}}_{ij},$$

In a forthcoming paper, focusing on the three-body problem, we use this formulation. Here we assume a uniform α for all bodies. This distinction is irrelevant in the case of two bodies.

$$m_i \ddot{\mathbf{r}}_i = - \sum_{j \neq i}^N \frac{G m_i m_j}{|\mathbf{r}_{ij}|^3} \mathbf{r}_{ij} + \sum_{j \neq i}^N \mathbf{f}_{\text{diss}}^{ij}(\dot{\mathbf{r}}_{ij}, \mathbf{r}_{ij}), \quad (12)$$

where the positions $\mathbf{r}_i \in \mathbb{R}^3$ for each mass m_i are relative to the center of mass.

2.1 Energy dissipation

To assess how the dissipative force (8) affects the system, we examine two conservative invariants of motion, namely the energy and angular momentum. Because the force is central, it immediately follows that the angular momentum (4) will remain conserved.

As for the energy, we can evaluate its dissipation by taking the scalar product of the equation of motion (12) with the velocity $\dot{\mathbf{r}}$

$$M \ddot{\mathbf{r}} \cdot \dot{\mathbf{r}} + \nabla_{\mathbf{r}} U(\mathbf{r}) \cdot \dot{\mathbf{r}} = -2\mathcal{D}(\dot{\mathbf{r}}, \mathbf{r}) \quad (13)$$

and identifying the left hand side as the derivative of the total energy $E = T + U$, and therefore

$$\frac{dE}{dt} = -2\mathcal{D} \leq 0. \quad (14)$$

Dissipation will only cease when $\mathcal{D} = 0$, which exclusively occurs in configurations of relative equilibria, or rotational central configurations, where the whole system rotates with all pairs \mathbf{r}_{ij} fixed.

In fact, the only case where dissipation can cease indefinitely is for two bodies. For $N = 2$, energy reaches its minimum at the circular relative equilibrium and remains there. Whenever other bodies are present, even if the movement is locally circular, the presence of any remaining body keeps $\mathcal{D} \neq 0$ at all times, unless they all rotate as a rigid body.

3 Central configurations

In this section we introduce some necessary concepts on central configurations (CCs) and analyze the effect of the dissipative force (8) on this family of orbits when restricted to the planar case. For further read on CCs, we direct the reader to Moeckel's work (Chap. 2 in [19]) on which we base our calculations.

Given a set of N -bodies with masses m_1, \dots, m_N , a CC is an arrangement where the force on each body constantly points towards the center of mass of the system, that is

$$\nabla U(\mathbf{r}) + \lambda \mathbf{M}(\mathbf{r} - \mathbf{c}) = 0, \quad (15)$$

for some constant $\lambda \in \mathbb{R}$. Here $\mathbf{r} \in \mathbb{R}^{3N}$ (or \mathbb{R}^{2N}) is the global state vector with all position coordinates for the N -bodies. The mass matrix

$$\mathbf{M} = \text{diag}_N(\mathbf{M}_i) = \begin{pmatrix} \mathbf{M}_1 & \mathbf{0} & \cdots & \mathbf{0} \\ \mathbf{0} & \mathbf{M}_2 & \cdots & \mathbf{0} \\ \vdots & \vdots & \ddots & \vdots \\ \mathbf{0} & \mathbf{0} & \cdots & \mathbf{M}_N \end{pmatrix} \in \mathbb{M}_{3N} \text{ (or } \mathbb{M}_{2N}\text{)},$$

stores the masses for each body, with $\mathbf{M}_i = m_i \mathbf{I}_3$ (or $m_i \mathbf{I}_2$), for $i = 1, \dots, N$. The vector $\mathbf{c} \in \mathbb{R}^{3N}$ is a stacked vector of the center of mass \mathbf{c}_0 , such that

$$(\mathbf{r} - \mathbf{c}) = (\mathbf{r}_1 - \mathbf{c}_0 \ \dots \ \mathbf{r}_n - \mathbf{c}_0),$$

with

$$\mathbf{c}_0 = \frac{1}{M} \sum_{i=1}^N m_i \mathbf{r}_i$$

as the center of mass in 3D (or 2D); $M = \sum_{i=1}^N m_i$ is the total mass. Normally \mathbf{c}_0 can be made zero if the coordinate reference frame is centered at it.

It can be shown that $\lambda = \frac{U(\mathbf{r})}{I(\mathbf{r})}$, where $I(\mathbf{r})$ is the moment of inertia of the system

$$I(\mathbf{r}) = (\mathbf{r} - \mathbf{c})^T \mathbf{M} (\mathbf{r} - \mathbf{c}) = \sum_{i=1}^N m_i |\mathbf{r}_i - \mathbf{c}_0|^2 = \frac{1}{M} \sum_{i=1}^N \sum_{j < i}^N m_i m_j r_{ij}^2. \quad (16)$$

3.1 Planar case

When restricted to a plane, the motion of any CC can be written in homographic form, combining a scaling of the configuration (homothetic motion) and a rotation (rigid body motion)

$$\mathbf{r}(t) - \mathbf{c}(t) = s(t) \mathbf{Q}(\theta(t)) (\mathbf{r}_0 - \mathbf{c}_0) \quad (17)$$

where $s(t) \in \mathbb{R}$ is the scaling factor, $\mathbf{Q}(\theta(t))$ is a rotation matrix perpendicular to the plane, such that each body is rotated equally by $\theta(t)$

$$\mathbf{Q}(\theta(t)) = \text{diag}_N(\mathbf{q}(\theta(t))) \in \mathbb{M}_{2N} \quad (18)$$

where

$$\mathbf{q}(\theta(t)) = \begin{pmatrix} \cos(\theta) & -\sin(\theta) \\ \sin(\theta) & \cos(\theta) \end{pmatrix} \in \text{SO}(2); \quad (19)$$

$(\mathbf{r}_0 - \mathbf{c}_0) \in \mathbb{R}^{2N}$ is the initial state of the CC. Note that $\mathbf{c}_0 \in \mathbb{R}^{2N}$ here generates an ambiguity with the vector $\mathbf{c}_0 \in \mathbb{R}^2$, denoting the position of the center of mass in the plane of motion. Although related, the ambiguity should not bring any conflict in the following calculations.

Over a homographic configuration $(\mathbf{r}_h, \dot{\mathbf{r}}_h)$ satisfying (17) the Rayleigh dissipation function (10) can be evaluated

$$\begin{aligned}\nabla_{\dot{\mathbf{r}}_i} \mathcal{D}(\mathbf{r}_h, \dot{\mathbf{r}}_h) &= \sum_{j \neq i}^N \mu_{ij} s^{-d} D(r_{ij,0}) \left\{ \dot{s} (\mathbf{q} \mathbf{r}_{ij,0}) \cdot (\mathbf{q} \hat{\mathbf{r}}_{ij,0}) + s \dot{\theta} \left(\frac{d\mathbf{q}}{d\theta} \mathbf{r}_{ij,0} \right) \cdot (\mathbf{q} \hat{\mathbf{r}}_{ij,0}) \right\} (\mathbf{q} \hat{\mathbf{r}}_{ij,0}) \\ \nabla_{\dot{\mathbf{r}}_i} \mathcal{D}(\mathbf{r}_h, \dot{\mathbf{r}}_h) &= \dot{s} s^{-d} \mathbf{q} \left(\sum_{j \neq i}^N \mu_{ij} r_{ij,0} D(r_{ij,0}) \hat{\mathbf{r}}_{ij,0} \right)\end{aligned}\tag{20}$$

where $\mu_{ij} = \alpha G m_i m_j$ and $D(r_{ij,0}) = |\mathbf{r}_{ij,0}|^{-d}$. When replacing the homographic form (17) into (10), the following identities were used

$$\begin{aligned}\frac{d(\mathbf{r} - \mathbf{c})}{dt} &= \left(\dot{s}(t) \mathbf{Q}(\theta(t)) + s(t) \mathbf{Q}' \dot{\theta}(t) \right) (\mathbf{r}_0 - \mathbf{c}_0) \\ \frac{d^2(\mathbf{r} - \mathbf{c})}{dt^2} &= \left(\ddot{s}(t) \mathbf{Q}(\theta(t)) + 2\dot{s}(t) \mathbf{Q}' \dot{\theta}(t) + s(t) \mathbf{Q}'' \dot{\theta}^2(t) + s(t) \mathbf{Q}' \ddot{\theta}(t) \right) (\mathbf{r}_0 - \mathbf{c}_0)\end{aligned}$$

where

$$\mathbf{Q}' = \frac{d\mathbf{Q}(\theta)}{d\theta} \rightarrow \frac{d\mathbf{q}}{d\theta} = \mathbf{j} \mathbf{q} \quad \text{with} \quad \mathbf{j} = \mathbf{q}(\pi/2),$$

and

$$\mathbf{Q}'' = \frac{d^2\mathbf{Q}(\theta)}{d\theta^2} \rightarrow \frac{d^2\mathbf{q}}{d\theta^2} = -\mathbf{q}.$$

It was also used that rotation matrices preserve inner products and that, being restricted to the plane they commute, implying

$$(\mathbf{j} \mathbf{q} \mathbf{r}_{ij,0}) \cdot (\mathbf{q} \hat{\mathbf{r}}_{ij,0}) = (\mathbf{j} \mathbf{r}_{ij,0}) \cdot \hat{\mathbf{r}}_{ij,0} = 0.$$

3.2 The special case $d = 3$

For $d = 3$, the dissipative force $\nabla_{\dot{\mathbf{r}}_i} \mathcal{D}$ in (20) can be expressed in terms of the gradient of the gravitational potential

$$\nabla_{\dot{\mathbf{r}}_i} \mathcal{D}(\mathbf{r}_h, \dot{\mathbf{r}}_h) = \alpha \dot{s} s^{-3} \mathbf{q} \nabla_{\mathbf{r}_i} U(\mathbf{r}_0).\tag{21}$$

From a mathematical perspective, it is interesting to consider the case $d = 3$ as it produces an additional symmetry between the dissipative and conservative terms. This equivalence allows us to obtain the equation for the homographic parameters $(s(t), \theta(t))$ in the presence of dissipation.

Substituting the homographic form (17) into the stacked equations of motion (12) for all bodies and multiplying by \mathbf{Q}^{-1} gives

$$\begin{aligned} \mathbf{M}(\ddot{\mathbf{r}}_h - \ddot{\mathbf{c}}) &= \nabla_{\mathbf{r}} U(\mathbf{r}_h) - \nabla_{\dot{\mathbf{r}}} \mathcal{D}(\mathbf{r}_h, \dot{\mathbf{r}}_h) \\ \left(\ddot{s} - s\dot{\theta}^2\right) \mathbf{M}(\mathbf{r}_0 - \mathbf{c}_0) + \left(2\dot{s}\dot{\theta} + s\ddot{\theta}\right) \mathbf{J}\mathbf{M}(\mathbf{r}_0 - \mathbf{c}_0) &= (s^{-2} + \alpha\dot{s}s^{-3}) \nabla_{\mathbf{r}_0} U(\mathbf{r}_0) \end{aligned} \quad (22)$$

where $\mathbf{J} = \text{diag}_N(\mathbf{j})$. To satisfy the CC condition, it must hold that

$$\nabla_{\mathbf{r}_0} U(\mathbf{r}_0) + \lambda \mathbf{M}(\mathbf{r}_0 - \mathbf{c}_0) = 0.$$

Simultaneously, since \mathbf{J} is a right-angle rotation, it renders $\mathbf{J}(\mathbf{r}_0 - \mathbf{c}_0)$ orthogonal to $(\mathbf{r}_0 - \mathbf{c}_0)$. This splits equation (22) into terms parallel and orthogonal to $(\mathbf{r}_0 - \mathbf{c}_0)$, yielding a system of equations for the coefficients

$$\begin{cases} \ddot{s} - s\dot{\theta}^2 = -\lambda (s^{-2} + \alpha\dot{s}s^{-3}) \\ s\ddot{\theta} + 2\dot{s}\dot{\theta} = 0 \end{cases} \quad (23)$$

Equation (23) is a dissipative Kepler-like system in the homographic parameters, with $s(t)$ playing the role of the radial coordinate and $\theta(t)$ the angular position. Due to this equivalence, the next section treats the two-body problem under dissipation with $d = 3$, providing solutions applicable both to the two-body case and to generic CCs for arbitrary N .

4 Two bodies

We describe the two-body system in polar coordinates (r, θ) , where $v = \dot{r}$ denotes the radial velocity. The equations of motion take the first-order form

$$\begin{cases} \dot{r} = v \\ \dot{v} = -\partial_r \mathcal{H} - \partial_v \mathcal{D} = \frac{C^2}{r^3} - \gamma \left(\frac{1}{r^2} + \alpha \frac{v}{r^3} \right) \end{cases} \quad (24)$$

with $\gamma = G(m_1 + m_2)$. The energy \mathcal{H} and dissipation \mathcal{D} functions are given by

$$\mathcal{H} = \frac{v^2}{2} + \frac{C^2}{2} - \frac{\gamma}{r} \quad \text{and} \quad \mathcal{D} = \frac{\alpha}{2} \frac{\gamma}{r^3} v^2, \quad (25)$$

and the (conserved) angular momentum C defined by

$$C = r^2 \dot{\theta}. \quad (26)$$

To solve the movement in equations (24), we proceed to a Poincaré compactification of the phase space in a series of transformations, following Dumortier et al. [20] (Chapter 5.1). The idea relies on mapping the infinite phase space $(r, v) \in [0, \infty) \times \mathbb{R}$ into a sphere, and analyze the dynamics at infinity via stereographic charts (planar

maps) covering the sphere. This allows us to understand the asymptotic behavior of solutions as they approach infinity in the original coordinates.

4.1 Poincaré compactification

We start by multiplying the equations in (24) by r^3 to produce a polynomial vector field, which preserves the phase space portrait of the system as it is equivalent to a time reparametrization:

$$\begin{cases} \dot{r} = r^3 v \\ \dot{v} = C^2 - \gamma(r + \alpha v), \end{cases} \quad (27)$$

The vector field (27) has two equilibria, namely the circular orbit

$$(r_c, v_c) = \left(\frac{C^2}{\gamma}, 0 \right), \quad (28)$$

and a second equilibrium

$$(r_e, v_e) = \left(0, \frac{C^2}{\gamma\alpha} \right), \quad (29)$$

which emerges as an artifact of the r^3 scaling and that does not exist in the conservative case for $\alpha = 0$ (Fig. 1 (A) and (B)).

The eigenvalues of the vector field (27) at the circular orbit (r_c, v_c) are

$$a_{\pm}^c = \frac{1}{2} \left(-\alpha\gamma \pm \sqrt{\alpha^2\gamma^2 - \frac{4C^6}{\gamma^2}} \right),$$

such that the orbit is an attracting node if $\alpha > \frac{2C^3}{\gamma^2}$, as $a_{\pm}^c < 0$, and an attracting focus if $0 < \alpha < \frac{2C^3}{\gamma^2}$, as $\text{Im}(a_{\pm}^c) \neq 0$ produces an oscillatory component (Fig. 1 (B)).

The dynamics around (r_e, v_e) is less clear. Restricting the vector field (27) over the line $r = r_e = 0$ implies a dynamic

$$\begin{cases} \dot{r} = 0 \\ \dot{v} = C^2 - \gamma\alpha v \end{cases}$$

Hence, the equilibrium (r_e, v_e) has an eigenvalue $a^e = -\gamma\alpha$ and a stable manifold coinciding with the axis $r = 0$. The other eigenvalue is zero and the associated center-manifold is tangent to the vector $(\alpha, -1)$ (Fig. 1 (C)).

The physical meaning of the equilibrium (r_e, v_e) is a direction towards which all orbits with initials conditions $(r(0), v(0))$, for fixed $v(0)$ and $r(0) > 0$ arbitrarily small, must approach before entering the circularization spiral towards (r_c, v_c) , as shown in Fig. 1 (B). In this figure, streamlines density and velocity close to $r = 0$ are much smaller than in the original dissipative Kepler problem (eq. 24).

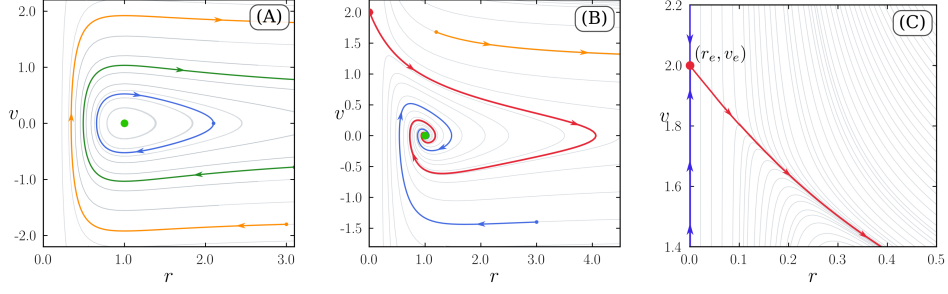


Fig. 1 Phase space portraits for the regularized two body system (eq. 27) for $C = \gamma = 1$. (A) The conservative case ($\alpha = 0$) showing elliptic (blue), parabolic (green), and hyperbolic (orange) orbits. (B) The system with dissipation ($\alpha = 0.5$) showing a captured orbit (blue), the weak-unstable-center manifold (red) from the equilibrium $(r_e, v_e) = (0, 2)$, and an escaping orbit (orange); the green dot marks the circular equilibrium $(r_c, v_c) = (1, 0)$. (C) Zoom of (B) near (r_e, v_e) ; stable branches along $r = 0$ are shown in blue.

To proceed and understand the dynamics at infinity we perform a Poincaré compactification of the vector field (27) introducing new variables (x, y) with the coordinate transform

$$(r, v) \mapsto (y, x) \quad \text{where} \quad r = \frac{1}{y}, \quad v = \frac{x}{y}$$

in a way that $y = 0$ corresponds to $r = \infty$. This corresponds to the U_1 chart in Dumortier et al. [20], pg. 151.

In the new coordinates, equation (27), after a new multiplication by y^3 becomes

$$\begin{cases} \dot{y} = -xy \\ \dot{x} = C^2 y^4 - x^2 - \gamma(1 + \alpha x)y^3 \end{cases} \quad (30)$$

The new system (30) has two equilibria: $(y_c, x_c) = (\frac{\gamma}{C^2}, 0)$, corresponding to the circular orbit, and

$$(y_\infty, x_\infty) = (0, 0)$$

corresponding to the limit as $r \rightarrow \infty$ with $v = \text{constant}$. As the linear approximation of (30) at $(0, 0)$ is null, (y_∞, x_∞) is a degenerate equilibrium. Thus, all unbounded solutions of the Kepler problem ($\alpha = 0$) are homoclinic to $(y_\infty, x_\infty) = (0, 0)$ (see Fig. 2 (A)).

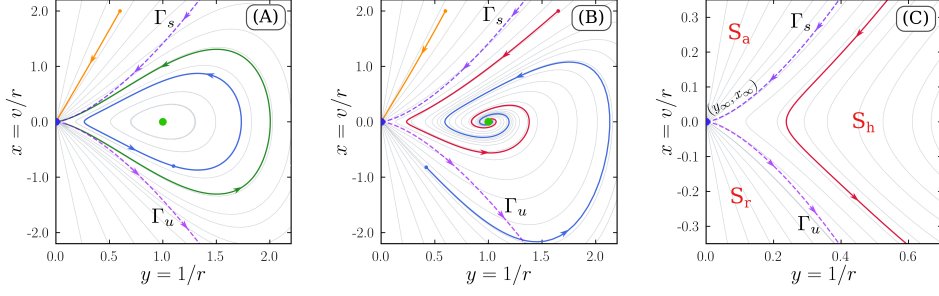


Fig. 2 Phase space portraits for the compactified system (30) for $C = \gamma = 1$. (A) The system without dissipation ($\alpha = 0$) showing elliptic (blue), parabolic (green), and hyperbolic (orange) orbits. The green dot is the circular orbit equilibrium $(y_c, x_c) = (1, 0)$. (B) The system with dissipation ($\alpha = 0.5$) showing a captured orbit (blue), and an escaping orbit (orange). The curve in red represents the weak-unstable-center manifold from the degenerate equilibrium (r_e, v_e) which here is a point at infinity. (C) Zoom of (B) near the degenerate equilibrium $(y_\infty, x_\infty) = (0, 0)$. The hyperbolic, attracting, and repelling sectors are denoted S_h, S_a , and S_r . The purple dashed lines $\Gamma_{u(s)}$ are local approximations to the unstable (stable) manifolds of $(y_\infty, x_\infty) = (0, 0)$.

Locally, the degenerate equilibrium (y_∞, x_∞) has a characteristic curve Γ_s approaching it for positive time, and a curve Γ_u approaching it for negative time. We can also divide the phase space x - y into three sectors: a hyperbolic sector S_h , an attracting sector S_a , and a repelling sector S_r (see Fig. 2 (C)).

To provide a local approximation to $\Gamma_{u(s)}$, we blow up the singularity (following [21], Sec. 1.2), by partially reverting the transformation $(y, x) \mapsto (y, v)$, where $v = \frac{x}{y}$. System 30 then becomes (after a division by y^2):

$$\begin{cases} \dot{y} &= -v \\ \dot{v} &= C^2 y - \gamma(1 + \alpha y v) \end{cases} \quad (31)$$

which is no longer singular at the origin, as $(\dot{y}, \dot{v})|_{(0,0)} = (0, -\gamma)$. Thus, for $|v|$ small

$$\frac{dy}{dv} = \frac{v}{\gamma(1 + \alpha y v) - C^2 y}$$

which has Taylor expansion near $(0, 0)$ as

$$y(v) = \frac{v^2}{2\gamma} + \mathcal{O}(v^4).$$

In the original variables (y, x) , we then have a local expression for the manifold branches

$$\Gamma_{u(s)} = x_{+(-)} = \pm \sqrt{2\gamma} y^{\frac{3}{2}}, \quad (32)$$

which does not depend on C or α .

For $\alpha = 0$, the vector field (30) has the first integral $\mathcal{H} = \frac{y^3(C^2y - 2\gamma) + x^2}{2y^2}$ (from eq. 25), and both characteristic curves Γ_u and Γ_s are determined by the equation $\mathcal{H} = 0$. One can check that this leads to the solution in equation (32).

In the Kepler problem, orbits with positive energy are asymptotically free, with $\mathcal{H} \rightarrow \frac{v^2}{2}$ as $t \rightarrow \pm\infty$. Scattering orbits in the dissipative or conservative scenarios are those for which the following two limits exist

$$\lim_{t \rightarrow -\infty} v(t) = -v_\psi < 0 \quad \text{and} \quad \lim_{t \rightarrow \infty} v(t) = v_\omega > 0.$$

In order to compute the asymptotic shape of a scattering orbit close to a point at infinity, one must solve

$$\mathcal{H} = \frac{y^3(C^2y - 2\gamma) + x^2}{2y^2} = \frac{v^2}{2} \quad \text{or} \quad y^3(C^2y - 2\gamma) + x^2 = v^2y^2$$

near $(y, x) = (y_\infty, x_\infty) = (0, 0)$. Up to leading order, the solution is

$$x = \pm v y + \mathcal{O}(y^{3/2})$$

Therefore, a scattering orbit leaves the point at infinity tangent to the line $x = -v_\psi y$, and arrives at the same point tangent to the line $x = v_\omega y$. In the presence of dissipation, $|v_\omega| < |v_\psi|$.

Besides, the equation for the characteristic curves $\Gamma_{u(s)}$, $x = \pm\sqrt{2\gamma}y^{\frac{3}{2}}$ implies that scattering orbits arrive and leave (x_∞, y_∞) tangent to the y -axis. Therefore, as expected, scattering orbits must both leave the point at infinity by the repelling sector S_r and arrive at the point at infinity in the attracting sector S_a (see Fig. 2 (C)).

To understand the dynamics at the remaining part of infinity, we will make use of a second chart to cover the points $(r, v) = (0, \pm\infty)$ (the U_2 chart in Dumortier [20], pg. 152). The change of variables from (27) in this case is

$$(r, v) \mapsto (w, z) \quad \text{where} \quad w = \frac{r}{v}, \quad z = \frac{1}{v}$$

In these coordinates, $z = 0$ corresponds to $v = \infty$.

After a convenient time reparametrization (again multiplying by z^3) the vector field (27) in the new chart becomes

$$\begin{cases} \dot{w} = w(w^2 + z^3(\gamma(w + \alpha) - C^2z)) \\ \dot{z} = z^4(\gamma(w + \alpha) - C^2z) \end{cases} \quad (33)$$

which has two equilibria: $(w_e, z_e) = (0, \frac{\alpha\gamma}{C^2})$, which corresponds to the (r_e, v_e) equilibrium previously found, and a new equilibrium

$$(w, z) = (w_{v\infty}, z_{v\infty}) = (0, 0)$$

representing the limit as $v \rightarrow \infty$ with $r = \text{constant}$. As the linear approximation to the vector field (33) at $(0, 0)$ is null, $(w_{v\infty}, z_{v\infty})$ is a degenerate equilibrium. The circular equilibrium (r_c, v_c) is mapped to infinity in this chart.

In Fig. 3 we show phase portraits for the system with and without dissipation. The mapping of orbits from (r, v) to (w, z) is not fully clear. Bounded orbits in (r, v) are mapped to a pair of curves in (w, z) that extend to infinity as any periodic orbit requires $v = 0$ that maps to $z, w \rightarrow \infty$. Consequently, a single initial condition (w_0, z_0) covers only one branch and is not able to reproduce the whole mapping of a bounded (r, v) orbit. The full periodic curve is recovered by gluing the two branches from the opposite quadrants ($w > 0, z > 0$) and ($w < 0, z < 0$). The remaining quadrants, ($w > 0, z < 0$) and ($w < 0, z > 0$) do not correspond to physical orbits, as in these regions $r < 0$ (see Fig. 3 (A)).

For $w = 0$ we have $\dot{w} = 0$ and $\dot{z} = \dot{z}(z)$, so the z -axis is invariant. In the presence of dissipation ($\alpha > 0$), the equilibrium (w_e, z_e) lies over the z -axis and there is a heteroclinic connection with $(w_{v\infty}, z_{v\infty})$. The unstable manifold of (w_e, z_e) (pink branches in Fig. 3 (B)) separates orbits of close approach with limited velocity (above the unstable branch), from those that can be arbitrarily close and reach infinite velocities (below the unstable branch).

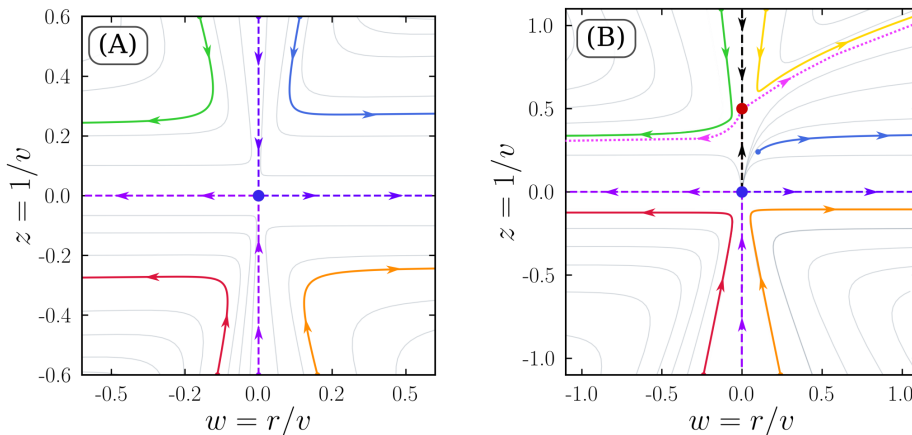


Fig. 3 Phase space portraits for the compactified system (33) for $C = \gamma = 1$. (A) The system without dissipation ($\alpha = 0$). Dashed lines show the stable and unstable manifolds for $(w_{v\infty}, z_{v\infty}) = (0, 0)$ and solid lines a few illustrative orbits. (B) The system with dissipation ($\alpha = 0.5$). The equilibrium point $(w_e, z_e) = (0, 0.5)$ divides the phase space, as indicated by its manifolds (dotted pink lines).

Finally, there is another chart (V_2 in [20], p. 152) that contains the limit $v \rightarrow -\infty$ with $r = \text{constant}$, which we denote $v_{-\infty}$. This point is also an equilibrium with the same local dynamics as that near $(w_{v\infty}, z_{v\infty})$. The vector field on this new chart is obtained by means of the change of variables $(w, z) \mapsto (-w, -z)$ in vector field (33) and multiplied by -1 , due to time reparametrization (last paragraph in pg. 152 of [20]).

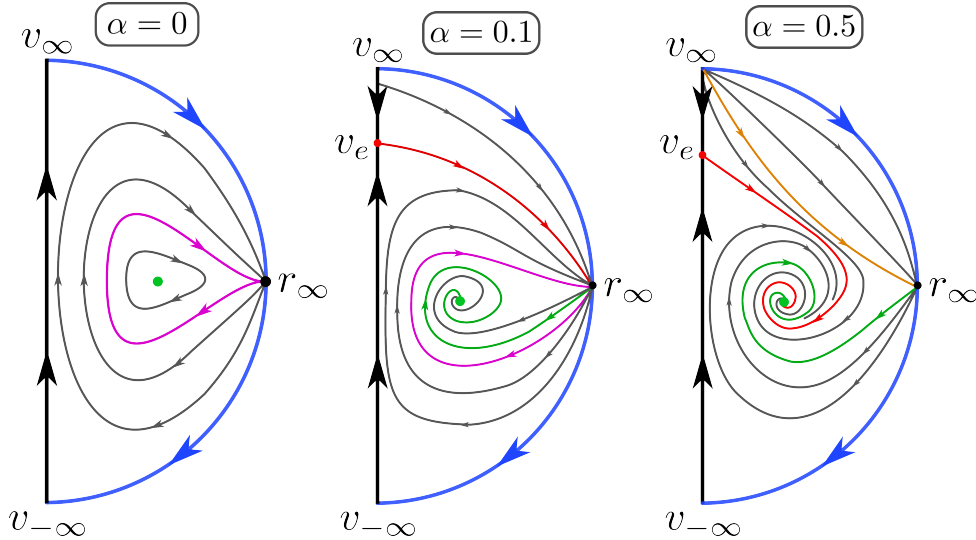


Fig. 4 Sketches of the phase space topology on the Poincaré disk for the Kepler system. Green dots mark the circular equilibrium (r_c, v_c) . (A) Conservative case ($\alpha = 0$) showing the parabolic separatrix (red). (B) Dissipative case ($\alpha = 0.1$) showing the separatrix and two center manifolds. (C) Dissipative case ($\alpha = 0.5$) showing a new ejection center manifold and the connection of the center manifold from (r_e, v_e) to (r_c, v_c) .

4.1.1 Phase portrait topology

To summarize, we recall that the initial vector field (24) describing the radial dynamics of the Kepler problem was regularized via a time rescaling (multiplication by r^3) yielding vector field (27). Since this vector field is polynomial, it admits a Poincaré compactification onto the disk, where only the half-disk with $r > 0$ is relevant to the analysis of the dissipative Kepler problem. The phase portrait topology of this half-disk was assembled from three different charts, each one obtained via local projections by compactification transforms.

To build the full phase portrait topology on the Poincaré disk, we considered three scenarios: $\alpha = 0$, $\alpha = 0.1$, and $\alpha = 0.5$, all for $C = \gamma = 1$ (see Fig. 4). The same topological results may be obtained for any other values of $C, \gamma > 0$.

For $\alpha = 0$, the global portrait is assembled from panels (A) of figures 1, 2, and 3. Figure 4 (A) shows the flow lines on the Poincaré half-disk, with a center at the circular orbit (r_c, v_c) , surrounded by periodic orbits (ellipses), together with parabolic and hyperbolic orbits that are homoclinic to the degenerate equilibrium at r_∞ . In this case the characteristic curves $\Gamma_{u(s)}$ from (y_∞, x_∞) merge (red curve), forming the separatrix between bounded and unbounded orbits.

For $\alpha = 0.5$, the global portrait is assembled from panels (B) of figures 1, 2, and 3. Figure 4 (C) shows the half-disk flow, where now a branch leaving (r_e, v_e) spirals toward the circular orbit (r_c, v_c) , which is now an attractor. A second branch connects scattering (escape) orbits that are not captured by the attractor.

For $\alpha = 0.1$, the phase portraits resemble those for $\alpha = 0.5$, except that Fig. 2 (B) is replaced by Fig. 5, where a transition half-way from the conservative to $\alpha = 0.5$ takes place. Here the separatrix is still present and coexists with the weak-center-manifold branch connecting r_∞ to the circular attractor. The difference from the case $\alpha = 0.5$ is that now three different regions appear in the phase space, as the weak-center-manifold from v_e connects to r_∞ , separating captured and scattered orbits. When $\alpha = 0.5$, this connection is lost, and only two regions appear, as the branch leaving v_e connects to the circular attractor. The global portrait for this case is shown in Fig. 4 (B).

The threshold between these two scenarios occurs for some $\alpha \in (0.1, 0.5)$, where the center-manifold of v_e merges to the characteristic curve Γ_s of r_∞ . At this point the scattering region disappears, with all incoming orbits ($v < 0$) being captured and lead to circularization. The basin of attraction of r_c increases along with α , as expected.

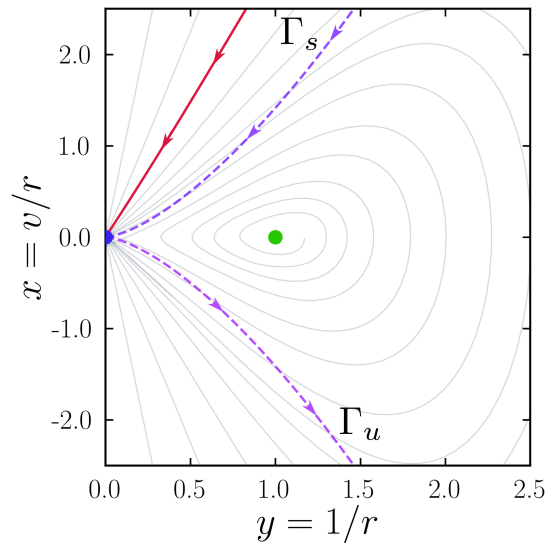


Fig. 5 Phase space portrait for the compactified system (30) for $C = \gamma = 1$ and $\alpha = 0.1$, showing that the weak-center-manifold, associated with $(r_e, v_e) = (0, 2)$, which in (y, x) is a point at infinity, is located within the S_a sector and connects to $(y_\infty, x_\infty) = (0, 0)$, instead of $(y_c, x_c) = (1, 0)$ as seen for $\alpha = 0.5$ (Fig. 2 (B) and (C)).

4.2 The angular-momentum-energy space

The angular-momentum-energy map, or CH map, is defined as the map that associates to each state $(\mathbf{r}, \mathbf{v}) \in \mathbb{R}^2/\{0\} \times \mathbb{R}^2$ of the dissipative Kepler problem the pair $(C = (\mathbf{r} \times \mathbf{v}) \cdot \hat{\mathbf{z}}, \mathcal{H}) \in \mathbb{R}^2$. For a given C , the minimum of $\mathcal{H} = \frac{v^2}{2} + \frac{C^2}{2r^2} - \frac{\gamma}{r}$ is achieved at the circular orbit, $r_c = \frac{C^2}{\gamma}$ and $v = 0$, with energy $\mathcal{H}_{\min} = -\frac{\gamma^2}{2C^2}$. Thus, the image of the CH map is the region above the graph in Fig. 6.

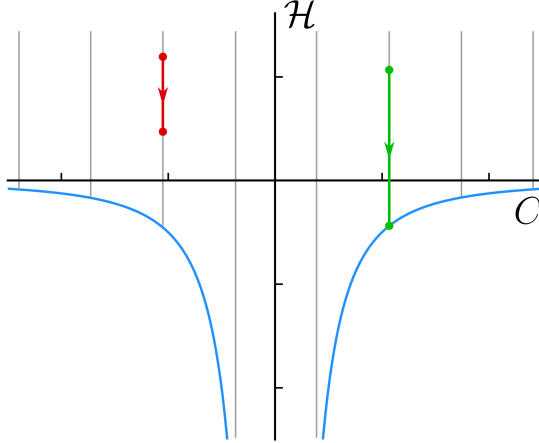


Fig. 6 Curve of minimum energy \mathcal{H} as a function of the angular momentum C , achieved at the circular orbit. Every orbit is mapped as a segment on the vertical lines above this curve. In green, an orbit captured by the circular attractor. In red, an example of a scattered (escape) orbit.

An orbit in the conservative Kepler system maps to a single point in the CH space, as C and \mathcal{H} are constants. In the presence of the dissipation considered here, however, the image of an initial point, not on the curve of minimum energy, always moves vertically down a line. There are two possibilities for this motion as $t \rightarrow \infty$. One, where the point moves vertically down till it reaches the minimum energy curve, which happens if, and only if, the initial point is in the basin of attraction of the circular orbit. The second possibility is that the point moves vertically down until reaching a limit with $\mathcal{H} > 0$. This scenario happens if, and only if, the initial point belongs either to the scattering region or to the escaping region.

Smale [1] provides a thorough analysis on this direction for the conservative case of systems with N -bodies.

5 Averaging

The goal in this Section is to average equations (24) with respect to the mean anomaly of the Kepler problem. We start by writing equations (24) in an intrinsic way as

$$i_X \omega_s = dH + Q \quad (34)$$

where X is the dissipative vector field. In the canonical set of variables (r, θ, \dot{r}, C) used in Section 4, the symplectic form is

$$\omega_s = dr \wedge d\dot{r} + d\theta \wedge dC,$$

and Q , which we will call dissipative one-form, is given by

$$Q = \alpha\gamma \frac{\dot{r}}{r^\beta} dr = \frac{\alpha\gamma}{2} \frac{\dot{r}}{r^{\beta+1}} d(r^2). \quad (35)$$

The angle θ is the true longitude that can be decomposed as

$$\theta = \varpi + f$$

with f as the true anomaly and ϖ as the longitude of the periapsis.

There is a canonical change of variables from (r, θ, \dot{r}, C) to the Delaunay variables [22] given by

$$\begin{aligned} M & \quad \Lambda = \sqrt{\gamma a} \\ \varpi & \quad \mathcal{H} = C = \Lambda\sqrt{1-e^2} = \Lambda\eta \end{aligned} \quad (36)$$

where: a is the semimajor axis, M is the mean anomaly, and Λ is the Delaunay action conjugated to M . In Delaunay's variables

$$\omega_s = dM \wedge d\Lambda + d\varpi \wedge dC, \quad H = -\frac{\gamma^2}{2\Lambda^2}$$

It remains to write the dissipative form $Q = \alpha\gamma \frac{\dot{r}}{r^\beta} dr$ in terms of the Delaunay variables.

In order to write the variables r and \dot{r} in terms of M , Λ , and the eccentricity e we will use the Hansen's expansions given by:

$$\left(\frac{r}{a}\right)^n e^{imf} = \sum_{k=-\infty}^{\infty} X_k^{n,m}(e) e^{ikM}, \quad (37)$$

where n , m , and k are integers and e is the eccentricity.²

The eccentricity can be written in terms of Λ and C , and therefore Q can be expressed in the Delaunay variables. However, the expression for the dissipative form becomes simpler if we replace C in Delaunay's variables by the eccentricity e . The set of variables (M, ϖ, Λ, e) is not canonical, so we must compute the symplectic form in this coordinates.

From equation (36) we obtain

$$dC = \sqrt{1-e^2} d\Lambda - \frac{e\Lambda}{\sqrt{1-e^2}} de = \eta d\Lambda - \frac{e\Lambda}{\eta} de$$

²The Hansen coefficients have the following properties:

$$X_k^{n,m} \in \mathbb{R}, \quad X_{-k}^{n,m} = X_k^{n,-m} \quad (38)$$

and

$$X_k^{n,m}(e) = e^{|m-k|} G_k^{n,m}(e^2) \quad (39)$$

where $G_k^{n,m}$ is analytic for $e^2 < 1$.

In the variables (M, ϖ, Λ, e) the symplectic form becomes

$$\omega_s = dM \wedge d\Lambda + \eta d\varpi \wedge d\Lambda - \frac{e\Lambda}{\eta} d\varpi \wedge de$$

As a result the dissipative Hamiltonian equations become:

$$\begin{pmatrix} \dot{M} \\ \dot{\varpi} \\ \dot{\Lambda} \\ \dot{e} \end{pmatrix} = \underbrace{\begin{pmatrix} 0 & 0 & 1 & \frac{\eta^2}{\Lambda e} \\ 0 & 0 & 0 & -\frac{\eta}{\Lambda e} \\ -1 & 0 & 0 & 0 \\ -\frac{\eta^2}{\Lambda e} & \frac{\eta}{\Lambda e} & 0 & 0 \end{pmatrix}}_{\mathbf{s}} \begin{pmatrix} \partial_M H + Q_M \\ \partial_{\varpi} H + Q_{\varpi} \\ \partial_{\Lambda} H + Q_{\Lambda} \\ \partial_e H + Q_e \end{pmatrix} \quad (40)$$

where $Q = Q_M dM + Q_{\varpi} d\varpi + Q_{\Lambda} d\Lambda + Q_e de$.

We use the Hansen's expansion to write³

$$\frac{\dot{r}}{r^{\beta+1}} = -\frac{d}{dt} \frac{r^{-\beta}}{\beta} = -\frac{1}{\beta} \frac{d}{dt} \left(a^{-\beta} \sum_{j=-\infty}^{\infty} X_j^{-\beta,0} e^{ijM} \right)$$

Since $\dot{a} = \dot{e} = 0$, $\dot{M} = n = \sqrt{\gamma} a^{-3/2}$, and $\Lambda = \sqrt{\gamma} a$, we obtain:

$$\frac{\dot{r}}{r^{\beta+1}} = -i \frac{\gamma^{\beta+2}}{\beta \Lambda^{2\beta+3}} \sum_{j=-\infty}^{\infty} j X_j^{-\beta,0} e^{ijM} \quad (41)$$

³Consider the Kepler vector field X given on a subset $U \subset \mathcal{R}^2 \times \mathcal{R}^2$, for instance, with coordinates (\mathbf{x}, \mathbf{v}) , where all orbits are elliptic. The elements $a, e, \varpi, C, r, v, f, \dots$ are functions defined on U . The vector field X acts on these functions as the time derivative, therefore

$$X \cdot r = \dot{r} = v, \quad X \cdot e = X \cdot a = 0, \quad X \cdot f = \dot{f} \dots$$

The Lie derivative of the differential of any function gives: $L_X dr = d(X \cdot r)X = d\dot{r}$, so the time derivative commutes with the differential.

In the coordinate system (M, Λ) , the vector field X is given by $X = n\partial_M$. We must be cautious in using the notation $X = n\partial_M$. For instance, if $F = F(r, M)$ then $\partial_M F(r, M)$ can be understood as the partial derivative of F with $r = \text{constant}$, which is false, since ∂_M means the derivative of the function while Λ is constant.

We again use Hansen's expansion to write

$$\begin{aligned}
dr^2 &= d \left(a^2 \sum_{k=-\infty}^{\infty} X_k^{2,0} e^{ikM} \right) = d \left(\gamma^{-2} \Lambda^4 \sum_{k=-\infty}^{\infty} X_k^{2,0} e^{ikM} \right) \\
&= i \gamma^{-2} \Lambda^4 \sum_{k=-\infty}^{\infty} k X_k^{2,0} e^{ikM} dM \\
&\quad + 4 \gamma^{-2} \Lambda^3 \sum_{k=-\infty}^{\infty} X_k^{2,0} e^{ikM} d\Lambda \\
&\quad + \gamma^{-2} \Lambda^4 \sum_{k=-\infty}^{\infty} (X_k^{2,0})' e^{ikM} de
\end{aligned} \tag{42}$$

where $(X_k^{2,0})' = \frac{d}{de} (X_k^{2,0})$.

Therefore, from equations (35), (41), and (42) we obtain

$$\begin{aligned}
dQ &= \frac{\alpha \gamma^{\beta+1}}{2\beta \Lambda^{2\beta-1}} \sum_{j=-\infty}^{\infty} \sum_{k=-\infty}^{\infty} j k X_j^{-\beta,0} X_k^{2,0} e^{i(k+j)M} dM \\
&\quad - 2i \frac{\alpha \gamma^{\beta+1}}{\beta \Lambda^{2\beta}} \sum_{j=-\infty}^{\infty} \sum_{k=-\infty}^{\infty} j X_j^{-\beta,0} X_k^{2,0} e^{i(k+j)M} d\Lambda \\
&\quad - i \frac{\alpha \gamma^{\beta+1}}{2\beta \Lambda^{2\beta-1}} \sum_{j=-\infty}^{\infty} \sum_{k=-\infty}^{\infty} j X_j^{-\beta,0} (X_k^{2,0})' e^{i(k+j)M} de
\end{aligned} \tag{43}$$

For $\alpha = 0$, equations (40) become $\dot{M} = n > 0$ and $\dot{\varpi} = \dot{\Lambda} = \dot{e} = 0$. This allows us to average the equations with respect to M .

We define the averaging operator

$$\langle h \rangle = \frac{1}{2\pi} \int_0^{2\pi} h(M) dM \tag{44}$$

Since the matrix \mathbf{S} in equation (40) does not depend on the mean anomaly the averaged equations become

$$\begin{pmatrix} \dot{M} \\ \dot{\varpi} \\ \dot{\Lambda} \\ \dot{e} \end{pmatrix} = \begin{pmatrix} 0 & 0 & 1 & \frac{\eta^2}{\Lambda e} \\ 0 & 0 & 0 & -\frac{\eta}{\Lambda e} \\ -1 & 0 & 0 & 0 \\ -\frac{\eta^2}{\Lambda e} & \frac{\eta}{\Lambda e} & 0 & 0 \end{pmatrix} \begin{pmatrix} \langle Q_M \rangle \\ \langle Q_\varpi \rangle \\ \partial_\Lambda H + \langle Q_\Lambda \rangle \\ \langle Q_e \rangle \end{pmatrix} \tag{45}$$

Equation (43) and $X_{-k}^{n,0} = X_k^{n,0}$ imply that the averaged components of the dissipative form are:

$$\begin{aligned}
\langle Q_M \rangle &= -\frac{\alpha\gamma^{\beta+1}}{2\beta\Lambda^{2\beta-1}} \sum_{k=-\infty}^{\infty} k^2 X_k^{-\beta,0} X_k^{2,0} \\
\langle Q_{\varpi} \rangle &= 0 \\
\langle Q_{\Lambda} \rangle &= 2i \frac{\alpha\gamma^{\beta+1}}{\beta\Lambda^{2\beta}} \underbrace{\sum_{k=-\infty}^{\infty} k X_k^{-\beta,0} X_k^{2,0}}_{=0} \\
\langle Q_e \rangle &= i \frac{\alpha\gamma^{\beta+1}}{2\beta\Lambda^{2\beta-1}} \underbrace{\sum_{k=-\infty}^{\infty} k X_k^{-\beta,0} (X_k^{2,0})'}_{=0}
\end{aligned} \tag{46}$$

Remark

$$\langle Q_M \rangle = \frac{1}{n} \underbrace{\langle 2\mathcal{D} \rangle}_{\langle \dot{E} \rangle} = \Delta E \geq 0 \tag{47}$$

where

$$\Delta E(a, e) = \frac{T}{2\pi} \int_0^{2\pi} \dot{E} dM = \int_0^T \dot{E} dt \tag{48}$$

is the energy dissipated in one period along an elliptic orbit with semi-axis a and eccentricity e .

Indeed

$$\begin{aligned}
\frac{(\mathbf{v} \cdot \hat{\mathbf{r}})^2}{|\mathbf{r}|^\beta} &= \frac{\dot{r}^2}{r^\beta} = -\frac{1}{2\beta} \frac{dr^2}{dt} \frac{dr^{-\beta}}{dt} = -\frac{1}{2\beta a^{\beta-2}} \frac{dr^2 a^{-2}}{dt} \frac{dr^{-\beta} a^\beta}{dt} \\
&= -\frac{1}{2\beta a^{\beta-2}} \frac{d}{dt} \left(\sum_j X_j^{2,0} e^{ijM} \right) \frac{d}{dt} \left(\sum_k X_k^{-\beta,0} e^{ikM} \right) \\
&= \frac{n^2}{2\beta a^{\beta-2}} \sum_{j,k} X_j^{2,0} X_k^{-\beta,0} jk e^{i(j+k)M}
\end{aligned}$$

Thus

$$\frac{1}{2\pi} \int_0^{2\pi} \frac{(\mathbf{v} \cdot \hat{\mathbf{r}})^2}{|\mathbf{r}|^\beta} dM = -\frac{n^2}{2\beta a^{\beta-2}} \sum_k X_k^{2,0} X_k^{-\beta,0} k^2$$

The result follows from equations (35) and (46).

In Figure 7 we show three plots of the function $-\sum_k k^2 X_k^{2,0}(e) X_k^{-\beta,0}(e)$ for $\beta = 2, 3, 8$. For constant values of a and e , this figure shows that the dissipation is stronger when β increases.

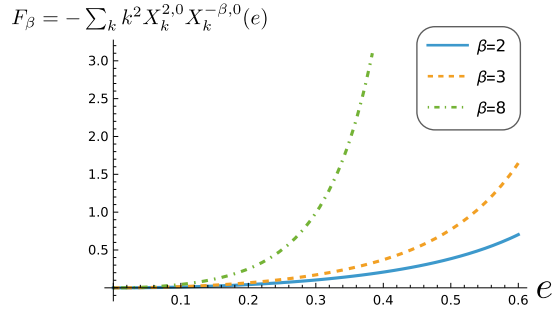


Fig. 7 The function $F_\beta(e) = -\sum_k k^2 X_k^{2,0} X_k^{-\beta,0}(e)$ for $\beta = 2, 3, 8$. The following expansions hold: $F_2(e) = e^2 + O(e^4)$, $F_3(e) = \frac{3e^2}{2} + O(e^4)$, and $F_8(e) = 4e^2 + O(e^4)$.

The averaged equations are $\dot{M} = n$, $\dot{\omega} = 0$ and

$$\begin{aligned} \dot{\Lambda} &= -\langle Q_M \rangle < 0 \\ \dot{e} &= -\frac{\eta^2}{\Lambda e} \langle Q_M \rangle < 0 \end{aligned} \quad (49)$$

Using $C = \Lambda\eta$ we obtain that C remains constant.

Note that $e = 0$ is an attracting equilibrium of the equation for \dot{e} . As $e \rightarrow 0$, the constancy of the angular momentum $C = \Lambda\sqrt{1-e^2}$ implies that $\Lambda \rightarrow C$. Therefore $a \rightarrow C^2/\gamma$ and the asymptotic value of a is determined by the initial angular momentum.

The Gauss form of the third Kepler law, namely,

$$a^3 n^2 = \frac{C^2}{\tilde{p}} = m$$

where $\tilde{p} = a(1-e^2) = a\eta^2$ is the semi-latus rectum, implies that the semi-latus rectum remains constant under the action of the dissipative force.

One may note that the semi-major axis is always decreasing, so the model cannot explain the Earth-Moon increasing distance but it can explain the Mercury-Sun decreasing distance.

6 Conclusion

We sought to understand the effect of a dissipative force that while removing energy preserves angular momentum. The force was motivated by a simplified tidal model for punctual masses, where the velocity dependence is linear and projected radially, making the force central. This form for the force preserves rotational symmetry while breaking time symmetry, and is trivially extendable to systems with any number of bodies.

In particular, we showed that a radial force whose dependence is homogeneous of degree $d = 3$ yields an extra ‘radial’ symmetry matching that of gravity. This allows us to easily derive the equations of motion for planar central configurations for generic N bodies, with the resulting system for its homographic parameters being equivalent to the dissipative Kepler problem.

In the derivation of these equations, if one is able to show that the central dissipative force can be expressed as a function of the gravitational potential for a generic degree of homogeneity, the techniques and results obtained here immediately follow for any value of d .

The global phase space portrait for the dissipative Kepler problem was obtained via a Poincaré compactification of the regularized vector field. The technique used relied on building three different charts to cover the Poincaré disk, where the dynamics near infinity can be analyzed locally.

The topology of flow lines in the dissipative Kepler system undergoes a transition as the dissipation strength increases, where the separatrix of bounded (captured) and unbounded (scattering) orbits in the conservative case reconnects with the weak-center-manifold (from (r_e, v_e)) linking to escaping orbits. This reconnection creates a new division between captured and scattered orbits, where all approaches between bodies are bounded and lead to circularization.

As mentioned above, the Kepler system corresponds to the homographic dynamics of any planar central configuration under dissipation. For sufficiently small dissipation and nonzero angular momentum, any such configurations in the circular equilibrium basins of attraction will have their homothetic (radial) motion damped. This leads any central configuration to purely rotational motion and therefore to a relative equilibrium. We showed that the circularization dynamics inside these basins are governed by a weak-center-manifold.

With the addition of bodies in the system ($N > 2$), the lack of a minimum to the energy changes the dynamics in the circularization attractor basin, as dissipation goes on forever and collisions may occur. Despite the rapidly growing complexity with the addition of bodies, even in the conservative case, the simpler two-bodies scenario may hint on the stabilization of orbits near large primaries for long periods of time.

To extend the current model, one could consider the effect of rotation of bodies, reintroducing some of the neglected tidal effects. Moreover, to increase flexibility, one may also assign different dissipation strengths amongst pairs of bodies, $\alpha \rightarrow \alpha_{ij} = \alpha_i \alpha_j$, adapting to realistic scenarios where the primary bodies respond differently to tides due to its inner structure.

Acknowledgements. This research was funded by the São Paulo Research Foundation (FAPESP) under grants 2024/15052-0 (M.L.) and 2023/07076-4 (C. R.).

C.R. thanks several colleagues with whom he discussed forces similar to the one considered in this paper: Claudio Asano, Lucas Ruiz, and especially Antonio Fernandes, who performed several computations on the dissipative Kepler problem in a different way that helped in understanding the problem.

Finally, we would like to acknowledge Prof. Mark Levi, who informed us about the PhD thesis of Chong Ai and for many interesting conversations on the subject of this paper and related topics.

References

- [1] Smale, S.: Topology and mechanics. i. *Inventiones mathematicae* **10**, 305–331 (1970) <https://doi.org/10.1007/BF01418778>
- [2] Contopoulos, G.: *Order and Chaos in Dynamical Astronomy*. Springer, ??? (2002)
- [3] Ferraz-Mello, S.: *Caos e Planetas: Dinâmica Caótica de Sistemas Planetários*. Editora Livraria da Física, São Paulo (2021)
- [4] Darwin, G.H.: On the bodily tides of viscous and semi-elastic spheroids, and on the ocean tides upon a yielding nucleus. *Philosophical transactions of the Royal Society* **170** (1879) <https://doi.org/10.1098/rstl.1879.0061>
- [5] Scheeres, D.J.: Minimum energy configurations in the n-body problem and the celestial mechanics of granular systems. *Celestial Mechanics and Dynamical Astronomy* **113**, 291–320 (2012) <https://doi.org/10.1007/s10569-012-9416-0>
- [6] Moeckel, R.: On central configurations. *Mathematische Zeitschrift* **1**(205), 499–517 (1990) <https://doi.org/10.1007/BF02571259>
- [7] Moeckel, R.: Minimal energy configurations of gravitationally interacting rigid bodies. *Celestial Mechanics and Dynamical Astronomy* **128**(1), 3–18 (2017) <https://doi.org/10.1007/s10569-016-9743-7>
- [8] Scheeres, D.J.: Stability in the full two-body problem. *Celestial Mechanics and Dynamical Astronomy* **83**, 155–169 (2002) <https://doi.org/10.1023/A:1020143116091>
- [9] Gabriel, T.S.J., Scheeres, D.J.: Energy dissipation end states of the sphere restricted planar three-body problem with collisional interaction. *Month Notices of the Royal Astronomical Society* **463**, 749–801 (2016) <https://doi.org/10.1093/mnras/stw1968>
- [10] Wang, S., Huang, G., Wu, X.: Simulations of dissipative circular restricted three-body problems using the velocity-scaling correction method. *The Astronomical Journal* **155**(67), 1–12 (2018) <https://doi.org/10.3847/1538-3881/aa9ff9>
- [11] Celletti, A.: Weakly dissipative systems in celestial mechanics. *Topics in Gravitational Dynamics. Lecture notes in physics* **729**, 67–90 (2007) https://doi.org/10.1007/978-3-540-72984-6_3
- [12] Celletti, A.: Some results on the global dynamics of the regularized restricted three-body problem with dissipation. *Celestial Mechanics and Dynamical Astronomy* **109**, 265–284 (2011) <https://doi.org/10.1007/s10569-010-9326-y>
- [13] Margheri, A., Ortega, R., Rebelo, C.: Some analytical results about periodic

- orbits in the restricted three body problem with dissipation. *Celestial Mechanics and Dynamical Astronomy* **113**, 279–290 (2012) <https://doi.org/10.1007/s10569-012-9415-1>
- [14] Ferraz-Mello, S., Ragazzo, C.G., Santos, L.R.: Dissipative forces in celestial mechanics. IMPA, Publicações Matemáticas: 30o Colóquio Brasileiro de Matemática (2015)
- [15] Goldreich, P., Peale, S.: Spin-orbit coupling in the solar system. *The Astronomical Journal* **71**(6), 425–437 (1966) <https://doi.org/10.1086/109947>
- [16] Meyer, A., Scheeres, D., Agrusa, H., Noiset, G., McMahon, J., Karatekin, O., Hirabayashi, M., Nakano, R.: Energy dissipation in synchronous binary asteroids. *Icarus* **391**, 115323 (2023) <https://doi.org/10.1016/j.icarus.2022.115323>
- [17] Ai, C.: Effect of tidal dissipation on the motion of celestial bodies. PhD thesis, The Pennsylvania State University (2012)
- [18] Mignard, F.: The evolution of the lunar orbit revisited. i. The Moon and the Planets **20**, 301–315 (1979) <https://doi.org/10.1007/BF00907581>
- [19] Llibre, J., Moeckel, R., Simó, C.: Central Configurations, Periodic Orbits, and Hamiltonian Systems. Springer, Basel (2015)
- [20] Dumortier, F., Llibre, J., Artés, J.C.: Qualitative Theory of Planar Differential Systems. Springer, Berlin (2006)
- [21] Arnold, V.I.: Geometrical Methods in the Theory of Ordinary Differential Equations, Volume 250. Springer, New York (2012)
- [22] Laskar, J.: Andoyer construction for Hill and Delaunay variables. *Celestial Mechanics and Dynamical Astronomy* **128**(4), 475–482 (2017) <https://doi.org/10.1007/s10569-017-9761-0>

